Theoretical Investigation of 2D Layered Materials as Protective Films for Lithium and Sodium Metal Anodes

Hongzhen Tian, Zhi Wei Seh, Kai Yan, Zhongheng Fu, Peng Tang, Yingying Lu, Ruifeng Zhang, Dominik Legut, Yi Cui, and Qianfan Zhang**

Rechargeable batteries based on lithium (sodium) metal anodes have been attracting increasing attention due to their high capacity and energy density, but the implementation of lithium (sodium) metal anode still faces many challenges, such as low Coulombic efficiency and dendrites growth. Layered materials have been used experimentally as protective films (PFs) to address these issues. In this work, the authors explore using first-principles computations the key factors that determine the properties and feasibility of various 2D layered PFs, including the defect pattern, crystalline structure, bond length, and metal proximity effect, and perform the simulations on both aspects of Li^+ (Na^+) ion diffusion property and mechanical stability. It is found that the introduction of defect, the increase in bond length, and the proximity effect by metal can accelerate the transfer of Li^+ (Na^+) ion and improve the ionic conductivity, but all of them make negative influences on the stiffness of materials against the suppression of dendrite growth and weaken both critical strains and critical stress. The results provide new insight into the interaction mechanism between Li^+ (Na^+) ions and PF materials at the atomic level and shed light onto exploring a variety of layered PF materials in metal anode battery systems.

1. Introduction

Rechargeable batteries with high capacity and long cycle life are of great demand for emerging applications including electric vehicles, grid storage, and advanced portable devices.[1–5] Recent efforts in this field have been focused on rechargeable batteries based on Li (Na) metal as the anode material, such as Li (Na)-S and Li (Na)-O_2 batteries.[6–10] The specific capacities of lithium and sodium metal can be up to 3860 and 1166 mA h g^{-1}, respectively, much higher than that of the graphite (372 mA h g^{-1}) in the traditional Li-ion batteries (LIB) and also higher than that of zinc, lead, and cadmium.[3,11,12] Therefore, Li (Na) metal can be viewed as a promising anode material candidate for the next-generation secondary batteries. Unfortunately, commercialization of the secondary Li (Na) metal battery still faces many challenges, including the volumetric change of Li (Na) metal during charging and the complex physical and chemical reactions at the interface between Li (Na) metal and electrolyte, resulting in low Coulombic efficiency and growth of dendrites.[13–16] As a result, it is critical to search for the suitable protective films (PFs) with high ionic conductivity and excellent mechanical performance, in order to improve the electrochemical properties and suppress dendrite formation.

Many strategies have been carried out to modify the nanoscale interphase between Li (Na) metal anode and electrolyte for improving performance of Li (Na) metal anode. Moreover, various kinds of external protection methods have developed including, inorganic or organic molecules coating, all-solid-state

H. Z. Tian, Dr. Z. H. Fu, P. Tang, Prof. R. F. Zhang, Prof. Q. F. Zhang
School of Materials Science and Engineering
Beihang University
Beijing 100191, P. R. China
E-mail: qianfan@buaa.edu.cn

Dr. Z. W. Seh
Institute of Materials Research and Engineering
Agency for Science, Technology and Research (A*STAR)
2 Fusionopolis Way, Innovis, Singapore 138634, Singapore

Dr. K. Yan, Prof. Y. Cui
Department of Materials Science and Engineering
Stanford University
Stanford, CA 94305, USA
E-mail: yicui@stanford.edu

Prof. Y. Y. Lu
State Key Laboratory of Chemical Engineering
College of Chemical and Biological Engineering
Zhejiang University
Hangzhou 310027, China

Prof. D. Legut
IT4Innovations Center
VSB-Technical University of Ostrava
17. listopadu 15, Ostrava CZ-70833, Czech Republic

Prof. Y. Cui
Stanford Institute for Materials and Energy Science
SLAC National Accelerator Laboratory
Menlo Park, CA 94025, USA

DOI: 10.1002/aenm.201602528

© 2017 WILEY-VCH Verlag GmbH & Co. KGaA, Weinheim

electrolytes, and alkaline ion additives.[17–22] Though these kinds of protection schemes can greatly improve performance of metal anodes, they can also suffer from the disadvantages such as low ionic conductivity at room temperature, large interfacial impedance, and large thickness. Recently, the novel lithium anode structure, using ultrathin 2D layered materials (hexagonal boron nitride (h-BN) or graphene) to cover the Cu current collector, was designed to form the 2D layer-Li-Cu sandwich structure,[23] which can effectively reduce interfacial reactions on the surface of lithium metal and suppress growth of lithium dendrites. As the stable interfacial layer, ultrathin 2D protective materials provide multiple advantages: (1) They are chemically stable against most chemicals in electrolyte; (2) Li^+ (Na^+) ions can diffuse through the layers with a short diffusion path due to their nano-even atomic-thickness; (3) Their mechanical strength is high enough to suppress growth of lithium dendrites; (4) Their stiffness is high enough to accommodate the deposition of lithium metal during charging; (5) In Li-S (Na-S) battery, the direct contact between the polysulfides and the lithium metal anode is prevented, and the undesired corrosion and shuttle effect by polysulfides can be effectively suppressed.

Due to the multifaceted requirements on the properties of PF, it is critical to carry out comprehensive theoretical study on both diffusion and mechanical performance for layered materials, in order to reveal the microscopic mechanism at the atomic level and design new types of PF materials to further improve the performance of metal anodes. Potential application of layered materials as energy materials has attracted broad interest, and much effort has been focusing on the electrochemical and physical properties of layered materials as electrode materials, including the Li storage, Li conductivity, etc. For example, Fan et al.[24] investigated the adsorption and diffusion of Li^+ ions on graphene with or without defect; Ford and co-workers[25] studied the adsorption and diffusion of Li^+ ion on 2D silicene and defective silicene; Wan and co-workers[26] explored the diffusion of Li through black and blue phosphorus sheet; several groups focused on the mechanical properties and strain–stress dependence on layered materials.[27–33] Despite the encouraging progress, theoretical studies of the effects of these layered materials are lagging behind and many issues remain unclear. First, great attention has been paid to lithium's intercalation and diffusion in electrode materials with high electronic conductivity, but people care little on the PF materials with insulating feature, such as h-BN. Second, the majority of research focuses on the use of layered materials as electrode materials instead of protective films, which require different properties, for example, the transition barrier or rate for vertical transfer instead of in-plane diffusion should be simulated in the case of protective films; Li^+ (Na^+) ion instead of Li (Na) neutral atom should be considered to simulate Li^+ (Na^+) in electrolyte; biaxial strain–stress dependence instead of uniaxial one should be investigated. Third, PFs are placed on the surface of metal, so the proximity effect on protective film induced by metal is very important, but this has rarely been considered in previous works. Due to slower progress on the Na-metal-based batteries, investigations on protective films for the Na metal anodes are few and far behind. Therefore, a systematic study on the diffusion characteristic of Li^+ (Na^+) ion across the vertical direction of h-BN, graphene, and other 2D materials is critically needed, in order to understand the mechanism at the atomic level and further optimize the performance of the protective film.

In the present work, we investigate the practicability of the typical 2D layered materials (h-BN, graphene, silicene, germanene, stanene, phosphorene, SnS, and SnSe) as protecting films for lithium metal anodes from aspects of both the diffusion and mechanical properties by first-principles calculations and focus on their relationship with the crystalline structures, defect feature, and metal's proximity effect. We will show that a different crystalline structure can induce different Li^+ (Na^+) ion diffusion and stiffness features, and the existence of defect and metal interface can improve the diffusion properties of Li^+ (Na^+) ion but impair the mechanical properties at the same time. Using the electronic structure computation and analysis scheme, we will explore the electronic origin of theoretical and experimental results of protective films and describe the interaction picture on this material system.

2. Method and Modeling

The first-principles calculations are performed based on density functional theory as implemented in the Vienna ab initio simulation package code.[34–36] We use projector augmented wave potential, while choose the generalized gradient approximation with the parametrization of Perdew–Burke–Ernzerhof to treat with the exchange correlation interaction.[37] The kinetic energy cutoff for plane wave expansion is set at 550 eV, which is enough for the 2D layered materials we select. A vacuum of 20 Å is used along the direction perpendicular to the layer to avoid slab's interaction with their periodic images. A Monkhorst–Pack mesh of $5 \times 5 \times 1$ is used for integration in reciprocal space. The calculations were performed with a $5 \times 3 \times 1$ supercell for graphene or h-BN, $4 \times 3 \times 1$ supercell for silicene, germanene, or stanene, $4 \times 4 \times 1$ supercell for phosphorene, SnSe, or SnS. To obtain the optimized structures, the forces on all atoms were minimized to be smaller than 0.01 eV $Å^{-1}$. In order to achieve the properties closely related to the protective function, both the diffusion and mechanical properties will be investigated. From the aspect of diffusion properties, the diffusion barriers and diffusion rates will be simulated, while from the aspect of mechanical properties, the Young's modulus, critical strain, and critical stress are extracted to evaluate the hardness or stiffness of the materials.

The PF materials we choose are single-layered hexagonal BN (h-BN), graphene, phosphorene, silicene, germanene, stanene, SnS, and SnSe. These materials are widely used in electrochemical applications, especially in the battery material system.[38–40] h-BN and graphene, as we have mentioned above, have already been applied as the PF material in the experiment and proved as good PF candidates.[23] Furthermore, these kinds of materials can also serve as the models of ultrathin layered materials with different structures: h-BN and graphene represent planar sp^2 materials; silicene, germanene, and stanene represent buckling sp^2–sp^3 hybrid materials; phosphorene, SnS, and SnSe represent puckered sp^3 materials. Beyond the pristine materials, the PF with various defect patterns, which have been shown to play an important role in metal ion's diffusion,[24,25,41] is investigated. For h-BN, the sheets with single B vacancy (SBV), single

© 2017 WILEY-VCH Verlag GmbH & Co. KGaA, Weinheim

N vacancy (SNV), and double B-N vacancy (BNV) are calculated, while for graphene, the sheets with single vacancy (SV), double vacancy (DV), and Stone–Thrower–Wales (STW) defect are calculated. The defect concentration we used is in the range of $\approx 10^{13}$ cm^{-2}, which is consistent with that in experiment.[23] For PF of Na anode, defective silicene, or phosphorene serves as the PF model. Here, we illustrate the crystalline structure of the materials in this study and different defect patterns as shown in Figure S1 (Supporting Information), and meanwhile, we list the bond length for different kinds of materials as shown in Table S1 (Supporting Information).

3. Results and Discussion

3.1. Diffusion and Properties

First, diffusion properties of Li^+ ion transferring through these PFs were explored, and the transfer barriers of single Li^+ ion passing perpendicularly through various 2D layered materials are computed by the climbing-image nudged elastic band (CI-NEB) method.[42] The CI-NEB is an improved algorithm of the traditional NEB method, which is more efficient on achieving the minimum energy path with linear interpolation of the diffusion coordinates (the diffusion coordination is the coordination involving cooperative motion of all atoms simultaneously, including both the Li^+ ion and the atoms in layered materials). To test the correction of the CI-NEB method, the diffusion barrier for proton-graphene system is calculated first, and the diffusion barrier we achieved is consistent with the previous study,[43] as shown in Figure S2 (Supporting Information). Then, the barriers for Li^+ ion penetrating through various PF materials are computed, and the energy profiles of Li^+ ion diffusion as a function of diffusion coordinate are exhibited in **Figure 1**a–d, while in Table S2 (Supporting Information), we show the calculated diffusion rate for Li^+ ion transferring through these materials at room temperature (300 K) on the basis of barrier values. Furthermore, in order to explore the temperature effect, we calculate and show the relation between diffusion rate and temperature for various h-BN and graphene materials in Figure S3 (Supporting Information). For pristine h-BN and graphene, the barriers are as high as 6.75 and 7.92 eV, respectively, indicating that it is very hard for Li^+ ion to diffuse through them. After introducing defect, the situation is fundamentally different. For h-BN, the sheet with SNV, SBV, and BNV defect can lead to much lower barriers of 2.84, 1.54, and 0.75 eV, respectively. The graphene sheets with SV, DV, and STW defect can lower the barriers to 3.60, 1.31, and 2.98 eV, respectively. The diffusion rates for Li^+ are in the range of 10^{-18}–10^{-52} cm^2 s^{-1}, more than 83 orders higher than pristine h-BN and graphene. This is also the reason why the defective h-BN and graphene can result in good performance as PFs. For h-BN, the SBV defect can induce faster Li^+ diffusion than SNV defect because of a much lower barrier, while the BNV can lead to the fastest diffusion among them. Compared with defective h-BN or graphene, the barrier magnitudes of pristine phosphorene (2.37 eV), silicene (1.39 eV), germanene (0.71 eV), stanene (0.17 eV), SnS (0.91 eV), and SnSe (0.86 eV) suggest that the Li^+ ion can diffuse through their interstitial sites with relatively higher permeability. The barrier values for defective graphene and silicene are similar to the ones from the previous report,[24,25,41] but the result for phosphorene differs,[26] probably because we adopt larger supercell for barrier simulations, which is also proved by previous work.[44] To guarantee that the size of the surface supercell we use is large enough, we calculated the relation between the diffusion barriers and the

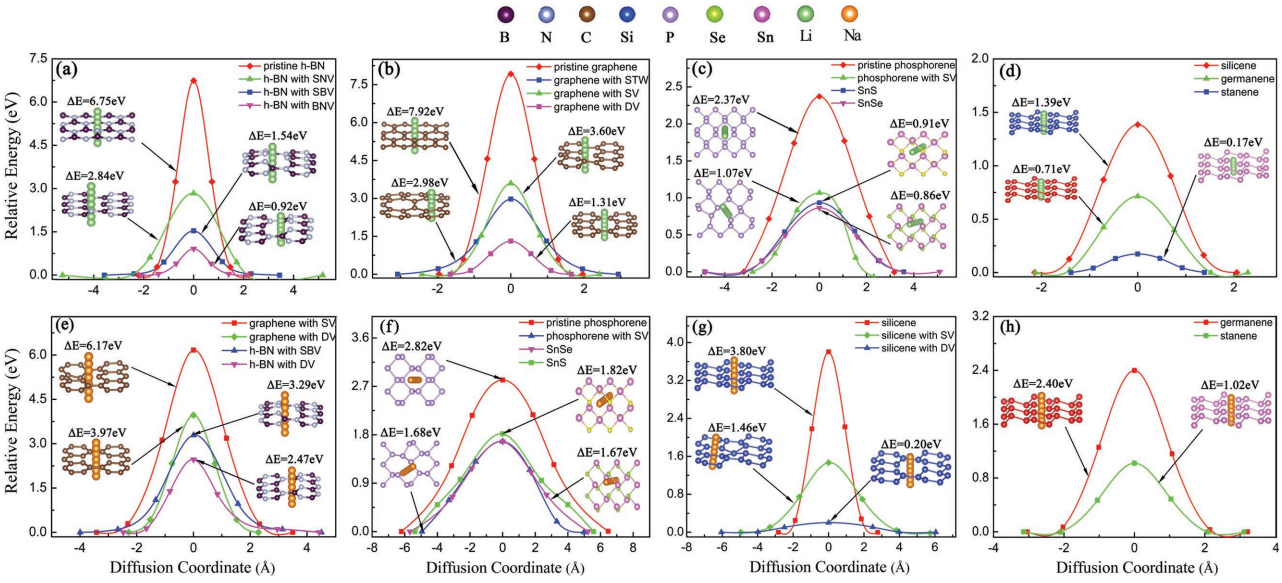

Figure 1. Potential-energy curves of Li^+ ion diffusion in the direction perpendicular to the sheet of a) h-BN and defective h-BN, b) graphene and defective graphene, c) phosphorene, defective phosphorene, SnSe, and SnS, d) silicene, germanene, and stanene. Potential-energy curves of Na^+ ion diffusion in the direction perpendicular to the sheet of e) defective graphene and defective h-BN, f) phosphorene, defective phosphorene, SnSe, and SnS, g) silicene and defective silicene, h) germanene and stanene. Schematic representations of diffusion paths are shown as the insets. Green and orange balls represent Li^+ and Na^+ ions, respectively. ΔE represents the corresponding diffusion barrier.

© 2017 WILEY-VCH Verlag GmbH & Co. KGaA, Weinheim

size of the supercell or the vacuum thickness in Figure S4a–d (Supporting Information). In addition, the influence of defect concentration was also studied and shown in Figure S4e,f (Supporting Information).

In general, the diffusion barrier has a strong dependence on the size of the hollow atomic ring pattern in the 2D layered materials, and it will decrease dramatically as the atomic bond length increases. But beyond that, other factors can also induce distinct barriers, which can be attributed to the electronic structures of different materials. This can be seen from the fact that the barriers induced by h-BNs are smaller (considering the SBV defect for single-atom vacancy) than their graphene counterparts with similar vacancy type. Although their structures and atomic bond lengths are almost the same (1.44 Å for h-BN and 1.42 Å for graphene), the h-BN with SBV can lead to better lithium conductivity compared to defective graphene (up to ≈24 orders of magnitude higher diffusion rate), which has been confirmed by experimental results.[23] It suggests that charge density distribution around the vacancy plays a very important role. We plot the charge density distribution for h-BN with SBV, SNV, and BNV defects and graphene with SV, STW and DV defects, as shown in **Figure 2**a–f. It can be clearly seen that the charge density around the vacancy is very small, which can greatly decrease the charge transfer from the film into Li^+ ion, reduce the electrostatic charge overlapping, and weaken the Coulombic interaction between Li^+ ion and 2D layered material, resulting in lower diffusion barriers of Li^+ ions. This is also the primary reason why defect can greatly accelerate the diffusion of Li^+ ion. In addition, line profiles of charge density between the center of defect hole and the neighboring atoms are quantitatively exhibited in Figure 2g,h. It can be seen that different defects result in different charge densities, and lower density corresponds to lower barrier, e.g., the charge density around the center of SBV defect (≈0.01 e $Å^{-1}$) is much lower than that around the center of SNV defect (≈0.05 e $Å^{-1}$) in h-BN, while the charge density magnitude around the center of SV defect in graphene (≈0.03 e $Å^{-1}$) lies between them. We also plot the charge density distribution and line profiles of charge density for various silicenes in Figure S5 (Supporting Information).

To further investigate the electronic interaction between Li^+ and PFs, Bader charges analysis was used to quantitatively calculate the charge transfer between Li^+ ion and the film. **Table 1** shows the charge state for Li^+ ions on stable site (e_S) and transition site (e_T) as well as the difference between them ($\Delta e = e_S - e_T$). It can be seen that the electron migrating to Li^+ on stable position is always lower than that on the transition point, which means the transfer from stable site to transition site is associated with the electron capture. To further demonstrate it, we extract graphene and defective graphene and plot the difference in charge density in Figure S6 (Supporting

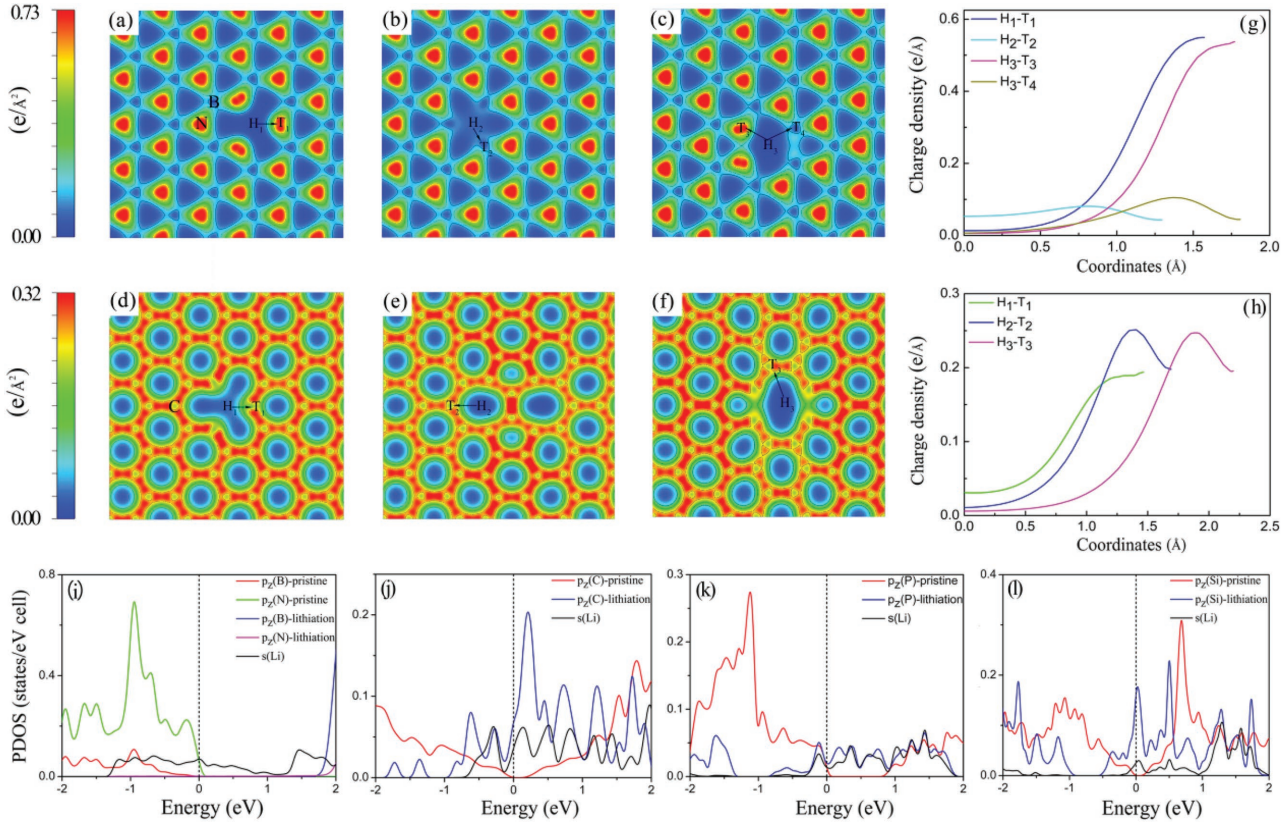

Figure 2. Charge density plots of a) h-BN with SBV, b) h-BN with SNV, c) h-BN with BNV, d) graphene with SV, e) graphene with STW defect, and f) graphene with DV. The red region represents charge accumulation and the blue one represents charge depletion. (g) and (h) show the line profiles of charge density between the center of hole and the neigboring atoms for defective h-BN and defective graphene, respectively, while the corresponding paths are marked in the charge density plot. Partial density of states for lithiated materials are shown as i) h-BN, j) graphene, k) phosphorene, and l) silicene. The zero energy (vertical dashed line) is set to the Fermi level.

© 2017 WILEY-VCH Verlag GmbH & Co. KGaA, Weinheim

Table 1. Li^+ and Na^+ ion charges were calculated by Bader charge scheme. e_S represents the charge on stable site. e_T represents the charge on transition site. Δe represents the charge difference between e_S and e_T ($\Delta e = e_S - e_T$). "–" means that the value has not been calculated because the corresponding barriers are too high to overcome by Li^+ (Na^+) ions.

	Li^+ [eV]	Li^+ ion charge [e]			Na^+ [eV]	Na^+ ion charge [e]		
	Barrier	e_S	e_T	Δe	Barrier	e_T	e_S	Δe
h-BN	6.75	+0.90	+0.58	0.32	–	–	–	–
h-BN with SNV	2.84	+0.87	+0.79	0.08	–	–	–	–
h-BN with SBV	1.54	+0.87	+0.80	0.07	3.29	+0.86	+0.73	0.13
h-BN with BNV	0.92	+0.87	+0.81	0.06	2.47	+0.87	+0.75	0.12
Pristine graphene	7.92	+0.90	+0.55	0.35	–	–	–	–
Graphene with STW	2.98	+0.90	+0.76	0.11	–	–	–	–
Graphene with SV	3.60	+0.89	+0.78	0.14	6.17	+0.87	+0.69	0.18
Graphene with DV	1.31	+0.90	+0.81	0.09	3.97	+0.88	+0.73	0.15
Phosphorene	2.37	+0.88	+0.75	0.13	2.82	+0.86	+0.77	0.09
Phosphorene with SV	1.07	+0.88	+0.81	0.07	1.68	+0.85	+0.77	0.08
SnS	0.91	+0.86	+0.82	0.04	1.82	+0.85	+0.75	0.10
SnSe	0.86	+0.86	+0.83	0.03	1.67	+0.84	+0.75	0.09
Silicene	1.39	+0.87	+0.73	0.14	3.80	+0.85	+0.65	0.20
Silicene with SV	–	–	–	–	1.46	+0.84	+0.73	0.11
Silicene with DV	–	–	–	–	0.20	+0.84	+0.75	0.09
Germanene	0.71	+0.87	+0.79	0.08	2.40	+0.84	+0.68	0.16
Stanene	0.17	+0.86	+0.82	0.04	1.02	+0.81	+0.71	0.10

Information), and it can be clearly seen that the charge transfers from graphene to Li^+ ion. In addition, the magnitude of Δe can almost determine the barrier height of lithium transport, and as Δe grows, the barrier will increase, which means that the electron capture is one of the most important mechanisms to hinder the transport of Li^+ ion. On the other hand, it also indicates that the crystalline structure has great influence on the diffusion, which can be seen from the fact that puckered materials induce larger barrier compared to buckling materials with similar bond length and similar electron migration amount, such as phosphorene versus silicene, SnS versus germanene, or SnSe versus stanene (see Table S1, Supporting Information, for the values of bond length). This can be mainly attributed to the different hybridization for buckling (sp^2–sp^3 hybrid) and puckered (sp^3) materials. The puckered materials have smaller bond angle due to sp^3 hybridization, which leads to smaller size of the hollow rings and enhance Coulomb interaction between Li^+ ion and 2D layered materials.[45]

The interface between PF and metal should also be considered. To this end, we calculate the diffusion energy evolutions at the interface by layered materials and investigate the proximity effect by metal. The study focuses on h-BN with SBV and SNV and graphene with SV, while three kinds of Li metal surfaces with the Miller indexes of ⟨100⟩, ⟨110⟩, and ⟨111⟩ are considered. We add multiple layers of Li atoms, with the thickness of no less than 10 Å (we show in Figure S7, Supporting Information, that such Li metal slab is thick enough), on one side of three kinds of defective PFs to build the interface model (the lattice mismatches with Li metal are no more than ≈1.5% and 1.0% for h-BN and graphene, respectively). We first calculated the formation energy for various junctions, which are summarized in Table S3 (Supporting Information). All of the formation energies are positive, which means these junctions are energetically stable, and strong interaction exists between PFs and metal. The energy profiles and corresponding barrier magnitudes are shown in **Figure 3**, while the conformations of PF-metal junctions and Li^+ ion transfer pathways are exhibited in Figure S8 (Supporting Information). After introducing the metal layers, the barriers for three kinds of PFs change into 0.75–0.89, 2.38–2.56, and 1.78–1.91 eV, respectively, and the diffusion path lengths also obviously change. That means the participation of metal surface can dramatically lower the diffusion barrier, which can greatly accelerate the diffusion of ions and improve the ion conductivity at the interface of the metal anodes. In Figure S9a–c (Supporting Information), we use the simplified interface model (adsorb one layer of Li atoms instead of adding multiple layers of Li atoms on the side of the 2D layered materials) to study the proximity effect on more kinds of PFs. The results for graphene with SV, phosphorene, and silicene reduce to 1.98, 1.32, and 1.26 eV, respectively, confirming again that the interface of the metal can lead to the reduction of barrier.

Such proximity effect can be mainly attributed to the reduction in bond strength and the increase in bond length in 2D layered materials induced by Li metal. Figure 2i–l shows the partial density of states (PDOS) for typical atoms in PFs (lithiated h-BN, graphene, silicene, and phosphorene) and Li atom. The strong overlapping between s orbital of Li adatom and the p orbital of the 2D layered materials' atoms indicates that the chemical bonds can be formed between the lithiated PF and Li

© 2017 WILEY-VCH Verlag GmbH & Co. KGaA, Weinheim

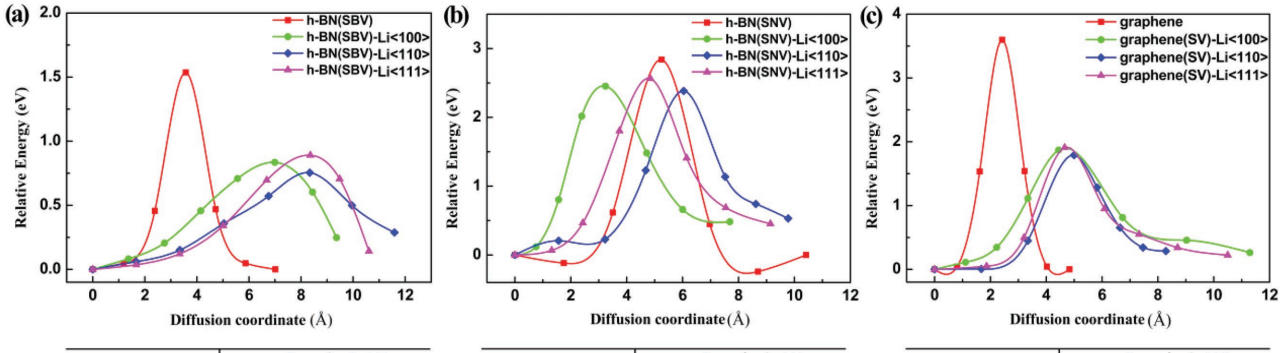

	Energy barrier (eV)
h-BN(SBV)	1.54
h-BN(SBV)-Li<100>	0.84
h-BN(SBV)-Li<110>	0.75
h-BN(SBV)-Li<111>	0.89

	Energy barrier (eV)
h-BN(SNV)	2.84
h-BN(SNV)-Li<100>	2.45
h-BN(SNV)-Li<110>	2.38
h-BN(SNV)-Li<111>	2.56

	Energy barrier (eV)
graphene(SV)	3.60
graphene(SV)-Li<100>	1.87
graphene(SV)-Li<110>	1.79
graphene(SV)-Li<111>	1.91

Figure 3. Comparisons on Li^+ ion diffusion through lithiated and unlithiated materials of a) h-BN with SBV, b) h-BN with SNV, and c) graphene with SV. Here, for each lithiated PF, Li metal surface with the Miller indexes of ⟨100⟩, ⟨110⟩, and ⟨111⟩ is considered. The energy barriers are listed in the corresponding below table.

metal and the binding interaction leads to the charge transfer between different materials and confirms again that there are remarkable interactions between 2D PFs and metal. As a result, the PDOS around Fermi-level increase and the electron fills the antibonding states with high energy, and according to the pseudo-gap theory,[46] the increase of electron density state around Fermi-level and the filling of antibonding state will weaken the bond strength inside PF. Therefore, the bond length will increase, and at the same time, the energy cost caused by the change of bond length or bond direction can be reduced by the softness of bond. All of these factors, originated from the electronic interaction between metal and PF, can decrease the barrier during Li^+ transfer. It can be also noticed that different Li surfaces can induce different barriers, and generally speaking, ⟨110⟩ surface can lead to the lowest one. This can be probably attributed to two aspects: first, different Li metal surface can induce different chemical potential on the Li^+ ion, which leads to different energy profile; second, ⟨110⟩ surface can provide the most Li atoms neighboring to the PFs (0.08, 0.11, and 0.08 atom $Å^{-2}$ for ⟨100⟩, ⟨110⟩, and ⟨111⟩, respectively), and according to analysis above, the softening effect can be the most remarkable one.

The transfer barriers of Na^+ ion through various 2D layered materials are also computed using similar scheme. Compared to Li^+ ion, the transfer barrier of Na^+ ion is significantly higher, mainly because the diameter of Na^+ ion (2.04 Å) is much bigger than that of Li^+ ion (1.52 Å), although their properties are quite similar (both are monovalent in nature). It can be seen from Figure 1e,g that it is much harder for Na^+ ion to diffuse through the sheet of graphene with SV and DV defects, h-BN with SBV defect, and pristine silicene compared with Li^+ transfer case, and the diffusion coefficients are ≈53, 45, 29, and 41 order lower, respectively. That is probably the reason that although h-BN or carbon materials can be used as the PFs for Li anode, their application in Na anodes has rarely been investigated. In contrast, the barrier magnitudes for pristine phosphorene (2.82 eV), phosphorene with SV (1.68 eV), silicene with SV (1.46 eV), and DV (0.20 eV), germanene (2.40 eV), SnSe (1.67 eV), and stanene (1.02 eV) indicate that Na^+ ion can diffuse through them with relatively high efficiency, as shown in Figure 1f–h. Particularly, the barrier of Na^+ ion through silicene with DV is only 0.20 eV and the corresponding diffusion coefficient can reach as high as 8.50×10^{-6} cm^2 S^{-1}. Therefore, it suggests that the PFs for Na metal anode should be prepared by materials with larger bond lengths or hollow atomic ring size, such as phosphorus or silicon with defects, germanium, and tin. According to the Bader charge analysis for Na^+ cases (as shown in Table 1), Na^+ can induce larger amount of electron transfer from the surrounding atoms compared with Li^+ (the difference is in the region of ≈0.06–0.12). Such enhancement on electron transfer is also an important reason that the transfer barrier for Na^+ is much higher.

To realize the protective function on metal anodes in Li-S battery, it is necessary to prevent large amounts of polysulfides from diffusing through the sheet. Here, we also calculate the diffusion barriers of S^{2-} ion passing through the sheet of silicene, germanene, and stanene. As shown in Figure S10 (Supporting Information), the diffusion barrier values for silicene, germanene, and stanene can reach up to 4.91, 3.42, and 2.18 eV, respectively, and the situated barrier for other 2D materials we choose should be higher because of smaller hole size. Compared with Li^+ ion, the diffusion coefficient of S^{2-} is almost ≈33 orders lower. Considering the sulfur materials are mainly in the state of long-chain polysulfides such as S_4^{2-} to S_8^{2-} instead of S^{2-} ion in electrolyte system, the process of polysulfide diffusion will be much more difficult. Therefore, the 2D materials we choose can efficiently prevent polysulfide or much bigger molecules in electrolyte from diffusing through the sheet while allow Li^+ ion to pass through easily.

3.2. Mechanical Stability

As a stable interfacial layer to protect Li (Na) metal anode, not only good diffusion properties but also excellent mechanical stability is required for 2D PFs. First, we calculate the Young's

© 2017 WILEY-VCH Verlag GmbH & Co. KGaA, Weinheim

Table 2. The calculated Young's moduli and critical strains for the 2D layered materials with and without defect. The values in parentheses represent the calculated Young's moduli for the corresponding lithiated materials.

	Young's moduli [GPa]		Critical strains	
	Zigzag	Armchair	Zigzag [%]	Armchair [%]
h-BN	831.4 (721.7)	829.7 (721.3)	20	20
h-BN with SBV	578.1	568.8	11	11
h-BN with SNV	767.6	766.8	12	12
h-BN with BNV	708.6	774.5	6	6
Pristine graphene	984.5 (843.4)	995.2 (841.8)	22	22
Graphene with SV	656.7	658.7	12	12
Graphene with DV	913.6	946.9	10	10
Graphene with STW	940.1	962.2	13	12
Phosphorene	166.0 (149.2)	37.1 (36.6)	15	21
Phosphorene with SV	164.6	35.4	10	10
SnS	42.1	18.9	13	9
SnSe	47.5	24.3	13	9
Silicene	178.9 (137.8)	177.6 (133.9)	16	16
Silicene with SV	145.8	162.3	13	15
Silicene with DV	163.1	170.4	6	13
Germanene	90.9 (89.2)	92.7 (90.0)	20	20
Stanene	62.2 (61.5)	62.2 (61.4)	21	21

modulus, in order to investigate the in-plane elastic stiffness. The values of Young's modulus are listed in **Table 2**. It indicates that all the materials we studied possess much higher Young's moduli than that of Li metal (≈4.9 GPa), and also higher than or comparable with common inorganic components in native solid electrolyte interphase (SEI) (e.g., ≈68 GPa for Li_2CO_3 and ≈65 GPa for LiF).[23] The values of Young's modulus for graphene and h-BN are as high as ≈1.0 TPa. As the bond length grows, the value of Young's modulus decreases dramatically, which can be attributed to the weakened bond formed by atoms with large radius. Unlike the isotropic Young's moduli of planar and buckling materials, puckered phosphorene, SnS, and SnSe exhibit anisotropic properties due to the anisotropic structure, and the modulus for zigzag direction is significantly higher than that in armchair direction. The lower Young's modulus in armchair direction can be attributed to the smaller alteration of the in-plane atomic crystalline structure under the same tensile stress and the tensile strain in the armchair direction is primarily induced by the stretching of the pucker. The calculated Young's moduli for h-BN, graphene, phosphorene silicene, and germanene in this study are consistent with those in previous work,[27,28,32] suggesting the validity of the results we achieved and the method we adopted.

Furthermore, it can be also seen from Table 2 that the introduction of defects can reduce the Young's moduli of 2D layered materials, while different types of defect can lead to different modulus. For h-BN, the Young's modulus for SBV defect is much smaller than that for SNV defect. For graphene, the Young's moduli for DV and STW defects are significantly larger than that of SV, which can be attributed to the reconstruction of crystal structure or reformatting chemical bonds of dangling bonds. The situations for defective phosphorene and defective silicene are similar to graphene and h-BN, which is due to the structure reconstruction. Hence introducing defect in phosphorene (defect concentration 5×10^{13} cm^{-2}) or silicene (defect concentration 4×10^{13} cm^{-2}) does not cause a large decrease of the Young's modulus, which is favorable for use in lithium batteries, especially as the PFs for the metal anode.[47]

Stiffness of 2D layered materials can be evaluated by critical strain (the strain at which ideal strength reaches). Equivalent tensile strains were simultaneously applied in the zigzag and armchair direction to investigate the critical biaxial strain. Such ideal strength sets up the upper limit of the material in reality and can also be applied to many materials in experiments, especially in the 2D materials.[32,43] It has been commonly believed that the force is mainly loaded by the in-plane stretching in 2D layered materials, so such modeling can simulate the limit of atomic bonds extension inside the materials and is applicable in studying various kinds of deformations in a micrometer or larger scale.[29,30,48] The applied strain is defined as $\varepsilon = \frac{a - a_0}{a_0}$, where a and a_0 are the lattice constants of strained and stable materials, respectively. Considering the 2D nature of the simulated material systems, the value of stress force achieved from simulations should be rescaled by Z/d_0 (Z is the cell length in the vacuum space direction and d_0 is the effective thickness of the systems),[32] in order to avoid the force being artificially averaged over the entire simulation cell including vacuum space and get the reasonable stress. Here, the strain–stress relations of these materials under equibiaxial loading were calculated and presented in **Figure 4**, and the value of critical strain is listed in Table 2. For the materials free from defect, the critical strains are in the region of 9%–22%. h-BN, graphene, germanene, and stanene possess relatively large critical strains among them (20%–22%), which indicates both strong and weak bonds can own good deformation tolerations. The results for graphene,[29] silicene,[30] or germanene[31] also agree well with the previous work. Compared with flat and buckling materials, puckered phosphorene, SnS, and SnSe show strong anisotropic properties. And all of them possess relatively low critical strain (considering the weaker direction), which means this series of materials is weak against the great external tensile. With the presence of defect, the situation can be quite different, and both the critical strain and the critical loading force will dramatically decrease, especially for h-BN and graphene (drop to 6%–12%). Therefore, the existence of defects can significantly impair the mechanical properties of these materials and should be avoided in PFs.

The proximity effect by Li (Na) metal also has a great effect on the mechanical performance of layered materials because of the interactions between the PFs and the metals. The study concentrates on both the Young's modulus and strain–stress relation. Due to distinct mechanical properties between PF and Li (Na) metal, the PF-metal junction model is not quite reasonable for the mechanical computation, instead, we put the Li (Na) adatom on one side of PF, with the hollow coverage of 33.33%, to imitate the effect by Li (Na) metal (the lithiated conformations are exhibited in Figure S11, Supporting

© 2017 WILEY-VCH Verlag GmbH & Co. KGaA, Weinheim

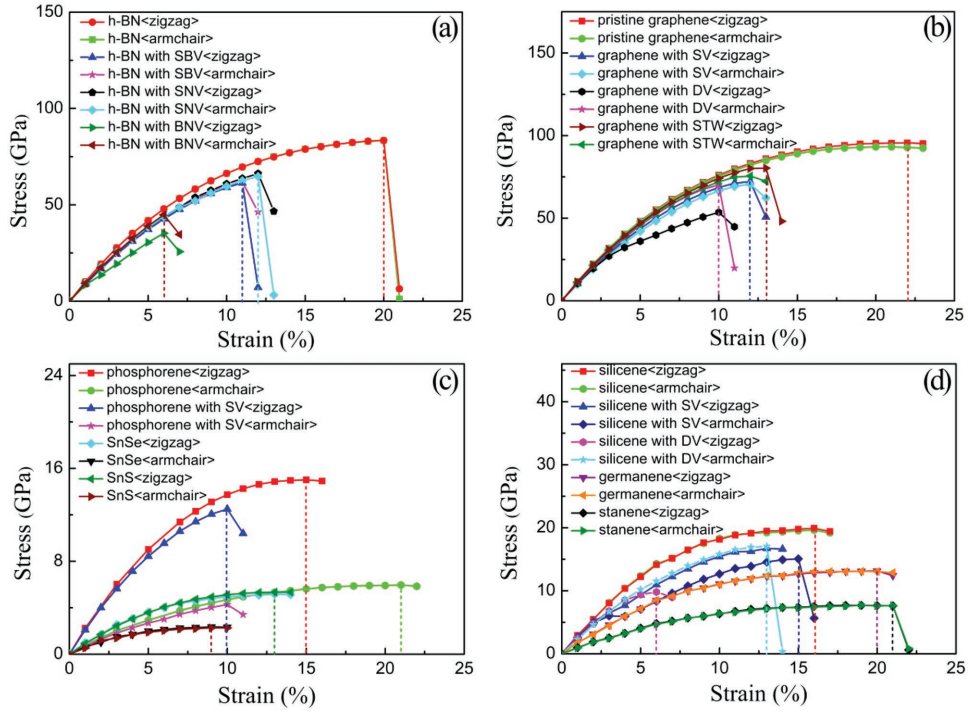

Figure 4. The strain–stress relations for a) h-BN and defective h-BN, b) graphene and defective graphene, c) phosphorene, defective phosphorene, SnSe, and SnS, and d) silicene, defective silicene, germanene, and stanene.

Information). The simulated Young's moduli for lithiated materials are listed in Table 2. Compared with the pristine layered materials, the in-plane stiffness of lithiated layered materials decreases by 1%–8%, demonstrating elastic softening of PF. In addition, we also estimate the moduli of PF neighboring with metal in Supporting Information (see Table S4, Supporting Information), which can further demonstrate this point. The strain–stress relations of lithiated and sodiated materials are shown in **Figure 5**. It can be clearly seen that for all the materials we choose, the participation of Li (Na) atoms can induce decrease in both critical strain and critical stress, which means that at the interface of Li or Na metal, the mechanical performance will become poor compared with the pristine materials. Relatively speaking, the h-BN and phosphorene experience sharp decrease of stiffness, while silicene experiences a minimal change of critical strain. In Figure S12 (Supporting Information), we show our simulation result on the dependence of strain–stress relation on Li concentration. It can be clearly seen that as the concentration of Li increases, the critical strain and critical stress decrease accordingly, and the mechanical performance grows poorer.

According to the analysis mentioned above, the participation of metal atoms and the interaction between PFs and metals can induce the charge transfer from metal atoms into PFs and cause the reduction in bond strength and the increase in bond length. Such bond softness is also the reason why lithiated (sodiated) PF possesses smaller Young's modulus and endures less force or strain compared with pristine ones. For silicene, germanene, and stanene, not only the bond length but also the buckling height will dramatically change. As shown in Figure S13a–c (Supporting Information), the value of buckling height sharply drops as the strain grows, in contrast to the gradual change in pristine PF materials, which means the buckling ring trend to become relatively flat under strains. In addition, we show the snapshots (side view) of the pristine and lithiated silicene at different applied tensile stress in Figure S13d (Supporting Information). The different variation tendency of buckling heights for pristine and lithiated system can be seen obviously. This strain mechanism does not exist in pristine PF materials but is induced by the participation of Li (Na) atoms. Such difference can also be seen from the fact that the stress–strain evolutions for lithiated (sodiated) silicene follow different tendency compared with their pristine counterparts when the strain is larger than ≈7%, as shown in Figure 5d–f. For lithiated silicene, the buckling height even drops to zero, which can provide a large tolerance for the horizontal extension of lattice. And this is the reason that the lithiated (sodiated) silicene can bear a similar strain with pristine material.

4. Discussion

Based on the simulation results above, it can be clearly seen that many factors can influence the protective effect of PF, including the defect pattern, crystalline structure, bond length and bond angle (or the ring size) and the metal proximity effect. According to the computation results, the introduction of defect, the increase of bond length and proximity effect have positive effects on the conductivity of Li^+ (Na^+) ion, which can induce lower diffusion barrier and higher diffusion rate. Conversely, all of them can have negative influence on hardness or stiffness of the materials, which is unfavorable for the

© 2017 WILEY-VCH Verlag GmbH & Co. KGaA, Weinheim

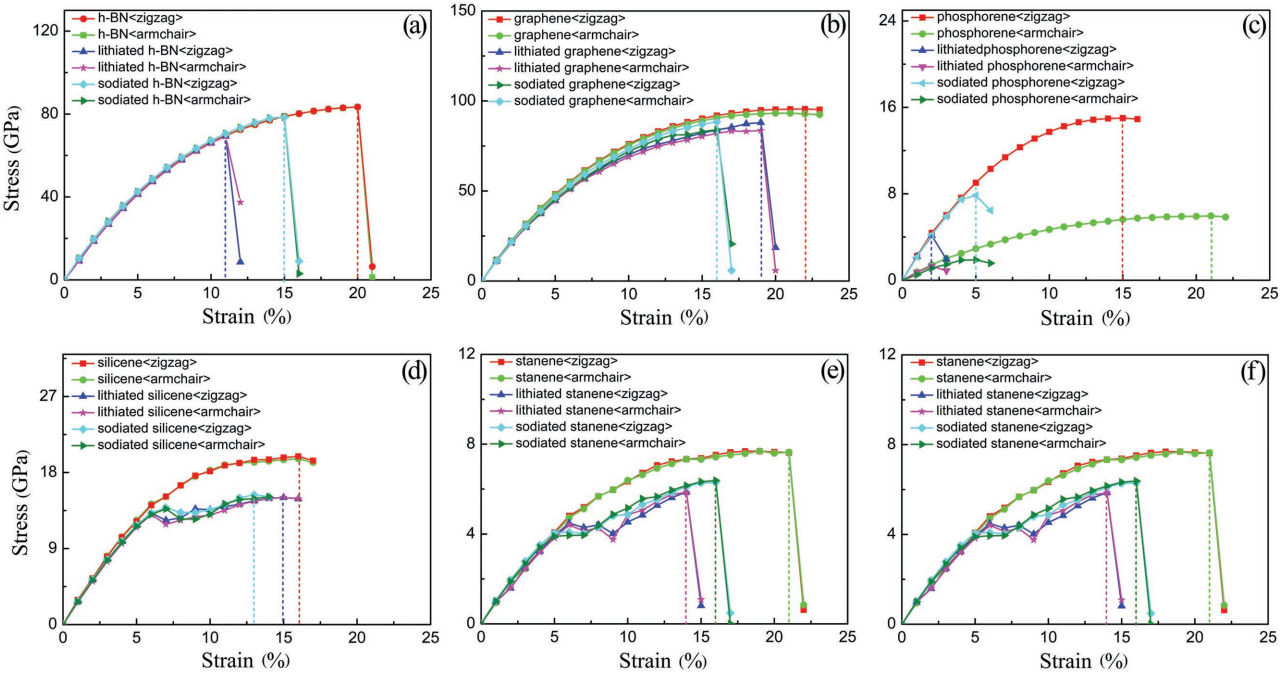

Figure 5. The comparison of strain–stress relations for a) h-BN, lithiated and sodiated h-BN, b) graphene, lithiated and sodiated graphene, c) phosphorene, lithiated and sodiated phosphorene, d) silicene, lithiated and sodiated silicene, e) germanene, lithiated and sodiated germanene, and f) stanene, lithiated and sodiated stanene.

suppression of lithium dendrites. Such a restriction makes it difficult to optimize both the diffusion and mechanical properties concurrently. Therefore, a balance should be struck between the considerations of ion conductivity and the stiffness against the lithium dendrites. From the comparison between different PF materials, it is suggested that the materials with puckering structure, such as phosphorene, SnS, and SnSe, are not good for the Li^+ (Na^+) diffusion, and even worse for the strain properties, which means that they are not suitable to be used as the PF materials on the metal surface.

According to our theoretical analysis, the studied effects can be mainly attributed to the electronic interaction and redistribution inside this material system. For example, the electron capturing is the essential parameter to determine the barrier height; the low electronic density around defect can lead to smaller resistance to Li^+ (Na^+) ion; the charge migration from metal into PF results in the filling of antibonding state and softens the covalent bind strength of PF, which is the origination of metal's proximity effect. Different kinds of PF materials possess different electronic structure features or bond characteristics. And as a result, distinct Li^+ (Na^+) diffusion behavior and distinct mechanical properties can be obtained.

Despite the similarity in electronic structure between the elements of Li and Na, the PF for Li anode, such as defective h-BN or graphene, may not be suitable for Na anode because the radius of Na^+ is much larger than that of Li^+, and the diffusion in these materials is much harder (the barriers we calculated are larger than 3 eV for two kinds of defective materials), which could lead to poor ionic conductivity. Therefore, searching for materials with longer bond length or larger ring size is necessary, at the cost of mechanical strength and the probability of corrosion by molecule or polysulfides from the electrolyte system. According to our simulation, silicene or Si materials are potentially promising PF for Na metal anode, with relatively high Na diffusion rate and stiffness stronger than common SEI films.

5. Conclusion

In summary, we investigated the practicability of h-BN, graphene, silicene, germanene, stanene, phosphorene, SnS, and SnSe as PFs for lithium or sodium anode by first-principles calculations. Our theoretical calculations indicate that the defect pattern, crystalline structure, bond length and bond angle (or the ring size), and metal proximity effect play the key role on the protective effect of PF from aspects of both the diffusion properties and mechanical performance, and all these effects can be mainly attributed to the electronic interaction or redistribution inside the material system. Introducing defect, increasing the size of hollow ring and the proximity effect can improve the conductivity of Li^+ (Na^+) ion, but all of them can have negative influence on hardness or stiffness of the materials against the suppression of lithium (sodium) dendrite growth. Therefore, it is important to strike a compromise between the considerations of ion conductivity and the stiffness against the lithium dendrites during the search for 2D-layered-structured materials as protective films. Our results not only provide new insight into the interaction mechanism between Li^+ (Na^+) ion and PF materials at the atomic level but also pave the way for the application of a variety of novel layered materials in metal anode battery systems.

© 2017 WILEY-VCH Verlag GmbH & Co. KGaA, Weinheim

Supporting Information

Supporting Information is available from the Wiley Online Library or from the author.

Acknowledgements

Q.F.Z. was supported by National Natural Science Foundation of China (11404017), Technology Foundation for Selected Overseas Chinese Scholar, Ministry of Human Resources and Social Security of China, and the program for New Century Excellent Talents in University (NCET-12-0033). Y.C. acknowledges the support of Battery Materials Research (BMR) Program under the Assistant Secretary for Energy Efficiency and Renewable Energy, Office of Vehicle Technologies of the U.S. Department of Energy. Z.W.S. was supported by the Institute of Materials Research and Engineering, Agency for Science, Technology and Research (A*STAR). R.F.Z. was supported by the Fundamental Research Funds for the Central Universities, National Natural Science Foundation of China (51471018), and National Thousand Young Talents Program of China. D.L. was supported by The Ministry of Education, Youth and Sports from the Large Infrastructures for Research, Experimental Development and Innovations project "IT4Innovations National Supercomputing Center—LM2015070." Y.L. acknowledges the financial support from MOST 2016YFA0202900 and the support from Chinese government under the "Thousand Youth Talents Program."

Received: November 15, 2016
Revised: December 23, 2016
Published online:

[1] M. Winter, R. J. Brodd, *Chem. Rev.* **2004**, *104*, 4245.
[2] M. Armand, J. M. Tarascon, *Nature* **2008**, *451*, 652.
[3] J. M. Tarascon, M. Armand, *Nature* **2001**, *414*, 359.
[4] P. G. Bruce, S. A. Freunberger, L. J. Hardwick, J. M. Tarascon, *Nat. Mater.* **2012**, *11*, 19.
[5] S. Chu, A. Majumdar, *Nature* **2012**, *488*, 294.
[6] Y. V. Mikhaylik, J. R. Akridge, *J. Electrochem. Soc.* **2004**, *151*, A1969.
[7] A. Manthiram, L. J. Li, *Adv. Energy Mater.* **2015**, *5*, 1401302.
[8] R. G. Cao, W. Xu, D. P. Lv, J. Xiao, J. G. Zhang, *Adv. Energy Mater.* **2015**, *5*, 1402273.
[9] W. Y. Li, H. B. Yao, K. Yan, G. Y. Zheng, Z. Liang, Y. M. Chiang, Y. Cui, *Nat. Commun.* **2015**, *6*, 7436.
[10] Y. M. Sun, N. Liu, Y. Cui, *Nat. Energy* **2016**, *1*, 16071.
[11] D. Linden, T. B. Reddy, *Handbook of Batteries*, Vol. *34*, McGraw-Hill, New York **2002**.
[12] M. S. Park, S. B. Ma, D. J. Lee, D. M. Lm, S. G. Doo, O. Yamamoto, *Sci. Rep.* **2014**, *4*, 3815.
[13] J. F. Qian, W. A. Henderson, W. Xu, P. Bhattacharya, M. Engelhard, *Nat. Commun.* **2015**, *6*, 6362.
[14] W. Xu, J. L. Wang, F. Ding, X. L. Chen, E. Nasybulin, Y. H. Zhang, J. G. Zhang, *Energy Environ. Sci.* **2014**, *7*, 513.
[15] S. S. Zhang, *J. Power Sources* **2013**, *231*, 153.
[16] E. Peled, *J. Electrochem. Soc.* **1979**, *126*, 2047.
[17] S. M. Choi, I. S. Kang, Y. K. Sun, J. H. Song, S. M. Chung, D. W. Kim, *J. Power Sources* **2013**, *244*, 363.
[18] K. G. Gallagher, S. Goebel, T. Greszler, M. Mathias, W. Oelerich, D. Eroglu, V. Srinivasan, *Energy Environ. Sci.* **2014**, *7*, 1555.
[19] G. Y. Zheng, S. W. Lee, Z. Liang, H. W. Lee, K. Yan, H. B. Yao, H. T. Wang, W. Y. Li, S. Chu, Y. Cui, *Nat. Nanotechnol.* **2014**, *9*, 618.
[20] A. C. Kozen, C. F. Lin, A. J. Pearse, M. A. Schroeder, X. G. Han, L. B. Hu, S. B. Lee, G. W. Rubloff, M. Noked, *ACS Nano* **2015**, *9*, 5884.
[21] G. Q. Ma, Z. Y. Wen, Q. S. Wang, C. Shen, J. Jin, X. W. Wu, *Mater. Chem. A* **2014**, *2*, 19355.
[22] F. Ding, W. Xu, G. L. Graff, J. Zhang, M. L. Sushko, X. L. Chen, Y. Y. Shao, H. M. Engelhards, Z. M. Nie, J. Xiao, X. J. Liu, P. V. Sushko, J. Liu, J. G. Zhang, *J. Am. Chem. Soc.* **2013**, *135*, 4450.
[23] K. Yan, H. W. Lee, T. Gao, G. Y. Zheng, H. B. Yao, H. T. Wang, Z. D. Lu, Y. Zhou, Z. Liang, Z. F. Liu, S. Chu, Y. Cui, *Nano Lett.* **2014**, *14*, 6016.
[24] X. F. Fan, W. T. Zheng, J. L. Kuo, *ACS Appl. Mater. Interfaces* **2012**, *4*, 2432.
[25] J. Setiadi, M. D. Arnold, M. J. Ford, *ACS Appl. Mater. Interfaces* **2013**, *5*, 10690.
[26] Q. F. Li, C. G. Duan, X. G. Wan, J. L. Kuo, *J. Phys. Chem. C* **2015**, *119*, 8662.
[27] H. Sahin, S. Cahangirov, M. Topsakal, E. Bekaroglu, E. Akturk, R. T. Senger, S. Ciraci, *Phys. Rev. B* **2009**, *80*, 155453.
[28] R. C. Andrew, R. E. Mapasha, M. A. Ukpong, N. Chetty, *Phys. Rev. B* **2012**, *85*, 125428.
[29] Y. Li, K. Yan, H. W. Lee, Z. D. Lu, N. Liu, Y. Cui, *Nat. Energy* **2016**, *1*, 15029.
[30] T. P. Kaloni, U. Schwingenschlögl, *Chem. Phys. Lett.* **2013**, *583*, 137.
[31] T. P. Kaloni, Y. C. Cheng, U. Schwingenschlögl, *J. Appl. Phys.* **2013**, *113*, 104305.
[32] Q. Wei, X. H. Peng, *Appl. Phys. Lett.* **2014**, *104*, 251915.
[33] Y. P. Ren, G. X. Cao, *Carbon* **2016**, *103*, 125.
[34] P. Hohenberg, W. Kohn, *Phys. Rev.* **1964**, *136*, B864.
[35] G. Kresse, J. Furthmüller, *J. Comput. Mater. Sci.* **1996**, *6*, 15.
[36] G. Kresse, J. Furthmüller, *Phys. Rev. B* **1996**, *54*, 11169.
[37] J. P. Predew, J. A. Chevary, S. H. Vosko, K. A. Jackson, M. R. Pederson, D. J. Singh, C. Fiolhais, *Phys. Rev. B* **1992**, *46*, 6671.
[38] J. Sun, H. W. Lee, M. Pasta, H. T. Yuan, G. Y. Zheng, Y. M. Sun, Y. Z. Li, Y. Cui, *Nat. Nanotechnol.* **2015**, *10*, 980.
[39] G. A. Tristaris, E. Kaxiras, S. Meng, E. G. Wang, *Nano Lett.* **2013**, *13*, 2258.
[40] J. J. Zhu, A. Chroneos, U. Schwingenschlögl, *Nanoscale* **2016**, *8*, 7272.
[41] F. Yao, F. Günes, Q. H. Ta, S. M. Lee, S. J. Chae, K. Y. Sheem, C. S. Cojocaru, S. S. Xie, H. Y. Lee, *J. Am. Chem. Soc.* **2012**, *134*, 8646.
[42] G. Henkelman, B. P. Uberuaga, H. Jónsson, *J. Chem. Phys.* **2000**, *113*, 9901.
[43] S. Hu, M. Lozada-Hidalgo, F. C. Wand, A. Mishchenko, F. Schedin, R. R. Nair, E. W. Hill, D. M. Boukhvalov, M. I. Katsnelson, R. A. W. Dryfe, I. V. Grigorieva, H. A. Wu, A. K. Geim, *Nature* **2014**, *516*, 227.
[44] Z. G. Wang, Q. L. Su, H. Q. Deng, W. D. He, J. H. Lin, Y. Q. Fu, *J. Mater. Chem. A* **2014**, *2*, 13976.
[45] S. Balendhran, S. Walia, H. Nili, S. Sriram, M. Bhaskaran, *Small* **2015**, *11*, 640.
[46] R. F. Zhang, D. Legut, Z. Lin, Y. S. Zhao, H. K. Mao, S. Veprek, *Phys. Rev. Lett.* **2012**, *108*, 255502.
[47] R. Dettori, E. Cadelano, L. Colombo, *J. Phys.: Condens. Matter* **2012**, *24*, 104020.
[48] T. S. Li, *Phys. Rev. B* **2012**, *85*, 235407.

© 2017 WILEY-VCH Verlag GmbH & Co. KGaA, Weinheim